NeuroImage 189 (2019) 71–84

Contents lists available at ScienceDirect

NeuroImage

journal homepage: www.elsevier.com/locate/neuroimage

Slow spindles are associated with cortical high frequency activity

Nasrin Sadat Hashemi [a], Fereshteh Dehnavi [a], Sahar Moghimi [a,b], Maryam Ghorbani [a,b,*]

[a] Department of Electrical Engineering, Ferdowsi University of Mashhad, Mashhad, 9177948974, Iran
[b] Rayan Center for Neuroscience and Behavior, Ferdowsi University of Mashhad, Mashhad, 9177948974, Iran

ARTICLE INFO

Keywords:
Sleep spindles
High frequency oscillations
Up and down states

ABSTRACT

Thalamocortical network shows self-sustained oscillations in a broad frequency range especially during slow wave sleep when cortical neurons show synchronized transitions between a quiescent down state and an active up state with beta and gamma oscillations. Inconsistent with previous models, thalamocortical spindles are separated into slow spindles (8_12 Hz) and fast spindles (13_17 Hz) with differential properties. We proposed that cortical high frequency (~ 25 Hz) activity during up states is the key ingredient for the generation of slow spindles. In fact, the nonlinear interaction between cortical high frequency and thalamic oscillations at fast spindle frequency reproduces oscillations in the range of the difference between the two frequencies that lies into the range of slow spindle. The developed simple deterministic thalamocortical model is able to reproduce up and down states with stochastic high-frequency up-state activity as well as both fast and slow spindles. In agreement with the previous experimental observations, the fast and slow spindles are generated at opposing phases of the up state. To further confirm the causal relationship between slow spindles and cortical high frequency oscillations, we next showed that externally applied high frequency stimulation enhanced the slow spindle activity. Moreover, the prediction of the model was validated experimentally by recording EEG from subjects during nap. Both model and experimental results show increase in high frequency activity before slow spindles. Our findings suggest the important role of cortical high frequency activity in the generation of slow spindles.

1. Introduction

Thalamocortical spindles are spontaneously generated waxing and waning oscillations during NREM sleep that are tightly linked to the processing of memories during sleep (Rasch and Born, 2013; Schabus et al., 2004). Recent studies have revealed the existence of two distinct types of sleep spindles, frontal slow spindles (8–12 Hz) and more posterior fast spindles (12–18 Hz) with different topographical distributions and relation to slow oscillations (SOs). Moreover slow and fast spindles have different pharmacological properties (Ayoub et al., 2013) and involve differently in memory consolidation during sleep (Barakat et al., 2011; Mednick et al., 2013) which further suggests two distinct mechanisms for the generation of slow and fast spindles (Timofeev and Chauvette, 2013). Slow oscillations are characterized by coherent repetitive transitions from a quiescent down state to a noisy up state of neurons over large section of the cortex. It has also been shown that high frequency oscillations in beta and gamma ranges (10–100 Hz) appear during the up state (Compte et al., 2008; Cox et al., 2014; Le Van Quyen et al., 2010; Steriade et al., 1996; Valderrama et al., 2012). Slow and fast spindles occur at opposing phases of up and down states; while slow spindles occur mainly during cortical up to down transition, fast spindles occur mostly in the beginning of the up state (Buzsaki, 2006; De Gennaro and Ferrara, 2003; Klinzing et al., 2016; Mölle et al., 2011). Up and down states have been observed in the cortical slices (Sanchez-Vives and McCormick, 2000) and there are strong evidences that fast spindles are triggered by the thalamus (Timofeev and Bazhenov, 2005). However, the origin of the slow spindles and their mechanism remain unknown. Multiple computational models have been proposed to reproduce the thalamocortical oscillations especially fast spindles and up and down states (UDS). Dendritic spike frequency adaptation (DSFA) and synaptic depression, have been proposed as possible mechanisms for the generation of up and down states in cortex (Ghorbani et al., 2012; Holcman and Tsodyks, 2006). Models considering bursting properties of thalamic neurons as well as the interaction between thalamic reticular (RE) nucleus and thalamocortical (TC) relay neurons are able to generate oscillations in the range of spindle frequency in isolated thalamus (Cona et al., 2014; Destexhe et al., 1996; Destexhe and Sejnowski, 2003). The interplay between thalamus and cortex has been taken into account in the

Abbreviations: SO, slow oscillation; UDS, up and down states; DSFA, dendritic spike frequency adaptation; HF, high frequency; SWS, slow wave sleep.

* Corresponding author. Department of Electrical Engineering, Ferdowsi University of Mashhad, Mashhad, 9177948974, Iran.
E-mail address: maryamgh@um.ac.ir (M. Ghorbani).

https://doi.org/10.1016/j.neuroimage.2019.01.012
Received 16 September 2018; Received in revised form 22 December 2018; Accepted 6 January 2019
Available online 9 January 2019

previous models to reproduce sleep oscillations especially spindle activity during SWS (Bazhenov et al., 2002; Cona et al., 2014; Costa et al., 2016; Destexhe and Sejnowski, 2003). However previous models are unable to explain different frequencies of slow and fast spindles and are inconsistent with recent findings.

We hypothesize that the nonlinear interplay between cortical high frequency oscillations and thalamus activity in the range of fast spindles can generate slow spindles. In fact the cortical neural network as a nonlinear system that receives one input (I_1) at frequency $f_1 \sim 13-17\ Hz$ in the range of fast spindle from the thalamus and another input (I_2) from cortex at higher frequency $f_2 \sim 20-30\ Hz$ is able to show oscillations at $f_2 - f_1$ (corresponding to $I_1 I_2$ that appears in the first nonlinear term in the Volterra series) which falls into the frequency range of the slow spindle (8–12 Hz). Therefore, in this model it is not required to consider a separate oscillator with frequency of slow spindles. To investigate this hypothesis, we propose a simple deterministic neural mass model consisting of one group of identical TC neurons, one group of identical RE neurons and two different cortical networks consisting of one identical group of excitatory and one identical group of inhibitory neurons representing two regions of the cortex. DSFA of excitatory cortical neurons and bursting properties of thalamic neurons are the key ingredients that enables the model to reproduce UDS and fast spindle respectively. In agreement with our hypothesis, the slow spindle is produced only in the cortical group with high frequency (HF) oscillations (20–30 Hz).

2. Methods

2.1. Model equations

2.1.1. Single thalamic cell model

The point neural firing rate model for thalamic cells consists of two variables, membrane potential, v_m (m equals to either t or r representing TC or RE neurons respectively) and a bursting variable, u_m, which is defined similar to a previous paper (Destexhe, 2009) but is modified to include nonlinear effects essential for a firing rate model.

$$\frac{dv_m}{dt} = -\frac{1}{\tau_m} v_m + \frac{f(u_m)}{A_m} + \frac{I_{in}}{A_m} f(u_m) = \frac{-f_m^{max}}{1 + exp\left(u_m + f_m^{th}\right)/\gamma_m)} \tag{1}$$

$$\frac{du_m}{dt} = \left[\frac{1}{\tau_m^u}(b_m - u_m)\right]. \tag{2}$$

$$if \quad v_r > 0\ mV \quad then \quad b_r = 0 \quad otherwise \quad b_r = -200 \quad mA$$

$$if \quad v_t \geq -0.1\ mV \quad then \quad b_t = 0 \quad otherwise \quad b_t = -200 \quad mA.$$

In Eq. (1), the first term on the right-hand side (RHS) represents the relaxation of the membrane potential to its equilibrium value with a relaxation time constant $\tau_m \sim 10\ ms$. The resting potential is assumed to be the same for all neuron types and all potentials is measured with respect to the common resting potential. A_m is the specific membrane capacitance and I_{in} represents the input current to the cell. The second term on RHS is proportional to a sigmoidal function of the bursting variable, u_m, considered to model T-type calcium currents which is essential for rebound bursting activity of thalamic neurons. When the cell is at rest or depolarized the equilibrium value of the bursting variable, b_m, is zero while it changes to a negative value when the cell is sufficiently hyperpolarized. When the cell is hyperpolarized, b_m changes to a negative value with large absolute value that results in decrease of u_m with a time constant of τ_m^u much larger than the membrane time constant (Izhikevich, 2007). The firing rate dependence on the membrane potential, $r(v_m)$, is different for tonic and burst modes of the neuron.

$$r(v_m) = \frac{R_m^T}{1 + exp\left(\left(v_m - v_m^T\right)/g_m^T\right)} e^{L_m u_m} + \frac{R_m^B}{1 + exp\left(\left(v_m - v_m^B\right)/g_m^B\right)}\left(1 - e^{L_m u_m}\right), \tag{3}$$

where L_m is a positive parameter that controls the sharpness of switch between the two modes. The first term on RHS represents the tonic mode and is dominant when the bursting variable is close to zero (note that the bursting variable can take only negative or zero values) while it goes to zero as the absolute value of u_m and so the second term representing the bursting mode increase. Here, R_m^T (R_m^B) is the maximal firing rate during tonic (burst) mode in a completely depolarized state while v_m^T (v_m^B) is the threshold firing potential. $g_m^T(g_m^B)$ shows the sharpness of the firing rate dependence on the membrane potential during tonic (burst) mode ($g_m^B \ll g_m^T$ *and* $F_m^B > F_m^T$). The parameters of Eqs. (2) and (3) are chosen to obtain results similar to the experimentally observed response of the TC and RE neurons to depolarizing and hyperpolarizing input currents in both tonic and burst modes (Fig. S1). The values of all the parameters of the model are shown in Table S1.

2.1.2. Thalamus

The thalamus is composed of one group of identical inhibitory neurons all with the same connectivity representing the reticular nucleus and one group of identical thalamocortical neurons again with the same connectivity. The number of TC and RE neurons (N_t and N_r respectively) are identical and equal to 500. The connection probability from RE to TC neurons, P_{rt}, is 4 time larger than the connection probability from TC to RE neurons, P_{tr} (Destexhe, 2009) and is twice the connection probability between RE neurons, P_{rr} (Cruikshank et al., 2010). The strengths of synaptic connections from neuron m to neuron n are given by the matrix elements J_{mn} which is negative for the inhibitory synapses and positive for the excitatory ones.

$$\begin{aligned}\frac{dv_r}{dt} &= -\frac{1}{\tau_r} v_r + \frac{f(u_r)}{A_r} + N_r P_{rr} J_{rr} r(v_r) + N_t P_{tr} J_{tr} r(v_t) \frac{dv_t}{dt} \\ &= -\frac{1}{\tau_t} v_t + \frac{f(u_t)}{A_t} + N_r P_{rt} J_{rt} r(v_r).\end{aligned} \tag{4}$$

The third and fourth terms on the RHS represent the rate of changes in the membrane potential due to EPSPs or IPSPs depending on the voltage-dependent firing rate of the presynaptic neuron.

2.1.3. Cortex

Cortex is modeled the same as our previous model (Ghorbani et al., 2012) which was based on dendritic spike frequency adaptation (DSFA), (Tsodyks and Markram, 1997). Only the excitatory-excitatory synapses are assumed to be subject to DSFA so that the synaptic connection between the cortical excitatory neurons, J_{ee}, is a sigmoid function of an adaptation variable c, that measures the degree of adaptation of the dendrites of the excitatory neurons to prolonged input.

$$J_{ee}(c) = \frac{J_{ee}(0)}{1 + \exp[(c - c^*)/g_c]}. \tag{5}$$

Here g_c, represents the width of the transition region and c^* shows the value of the adaptation parameter where the synaptic strength has dropped by a factor of 2 from its maximum value $J_{ee}(0)$. The mean adaptation level of an excitatory neuron, c increases from its equilibrium value (set to be zero) as the excitatory neuron receives inputs from other excitatory neurons and decays slowly to zero in the absent of excitatory inputs.

$$\frac{dc}{dt} = -\frac{1}{\tau_c} c + \Delta c \sum_m r_e^m\left(v_e^m\right). \tag{6}$$

The adaptation recovery time τ_c is taken to be 500 ms (Ghorbani et al., 2012). The sum on the RHS is over the excitatory neurons that make a synaptic junction with the neuron. Δc shows the increase of the mean

adaptation parameter per incoming action potential.

Cortical network consists of two weakly coupled network pairs each of them is composed of one group of identical excitatory neurons (EX) and one group of identical inhibitory neurons (IN). The two networks have the same number of neurons and the number of excitatory neurons, $N_e = 8000$ is 4 times larger than the number of inhibitory neurons, $N_i = 2000$. The synaptic strengths and variables of network 2 are indicated by primes. Within each network all the possible connections, i.e. the synaptic connection from excitatory to excitatory neurons, J_{ee}, from inhibitory to inhibitory neurons, J_{ii}, from excitatory to inhibitory neurons, J_{ei} and from the inhibitory to excitatory neurons, J_{ie} are considered. For the connections between the two networks, only long-range excitatory to excitatory connections with the synaptic strength J_{ee}^{coup} and excitatory-inhibitory connection with synaptic strength J_{ei}^{coup} are included. The firing rate of the neuron, $r(v_m)$ (m equals to either e or i representing cortical excitatory and inhibitory neurons respectively) is a sigmoid function of the membrane potential,

$$r(v_m) = \frac{r_{max}}{1 + \exp(-(v_m - v^*)/g_m)}. \tag{7}$$

Here, r_{max} ~70 Hz is the maximal firing rate in a completely depolarized state while v^* is the threshold firing potential and g_m shows the sharpness of the firing rate dependence on the membrane potential.

Previously we have shown that the frequency of oscillations during up state for a uniform network of excitatory and inhibitory neurons can be approximated as below (Ghorbani et al., 2012):

$$\Omega \approx \frac{1}{\tau_i}\sqrt{\left[\frac{\tau_i}{\tau_e} - \left(\frac{g_i}{g_e}\right)\frac{J_{ee}(c)}{J_{ei}}\right]\left(1 + \frac{|J_{ii}|J_{ee}(c)}{J_{ei}|J_{ie}|}\right) + \left(\frac{J_{ee}(c)}{J_{ei}}\right)\left(\frac{g_i}{g_e}\right)}. \tag{8}$$

2.2. Thalamocortical network

In the full model that consists of both thalamus and cortex, TC neurons project to excitatory and inhibitory neurons of the two cortical networks and cortical excitatory neurons project to TC and RE neurons. J_{te}, $J_{te}^{'}$, J_{et} and $J_{et}^{'}$ denote respectively synaptic connection from TC to EX, from TC to EX', from EX to TC and from EX' to TC. Similarly P_{mn} shows the connection probability from neuron m to neuron n where m and n can be equal to e, i, r and t representing cortical excitatory, cortical inhibitory, thalamic reticular and thalamocortical neurons respectively. The full model is described by 10 rate equations:

$$\frac{dv_e}{dt} = -\frac{1}{\tau_e}v_e + N_e P_{ee} J_{ee}(c) r(v_e) + N_i P_{ie}\, J_{ie} r(v_i) + N_e P_{ee}^{coup}\, J'^{coup}_{ee}(c) r(v_e') + N_t P_{te}\, J_{te} r(v_t)$$

$$\frac{dv_i}{dt} = -\frac{1}{\tau_i}v_i + N_i P_{ii}\, J_{ii}\, r(v_i) + N_e P_{ei}\, J_{ei}\, r(v_e) + N_e P_{ei}^{coup} J'^{coup}_{ei}\, r(v_e') + N_t J_{ti} r(v_t)$$

$$\frac{dc}{dt} = -\frac{1}{\tau_c}c + N_e P_{ee} \Delta c\, r(v_e) + N_e P_{ee}^{coup} \Delta c\, r(v_e')$$

$$\frac{dv_e'}{dt} = -\frac{1}{\tau_e}v_e' + N_e P_{ee} J_{ee}'(c') r(v_e') + N_i P_{ie} J_{ie}' r(v_i') + N_e P_{ee}^{coup}\, J_{ee}^{coup}(c') r(v_e) + N_t P_{te} J_{te}' r(v_t)$$

$$\frac{dv_i'}{dt} = -\frac{1}{\tau_i}v_i + N_i P_{ii} J_{ii}' r(v_i') + N_e P_{ei} J_{ei}' r(v_e') + N_e P_{ei}^{coup} J_{ei}^{coup} r(v_e) + N_t P_{ti} J_{ti}' r(v_t)$$

$$\frac{dc'}{dt} = -\frac{1}{\tau_c}c' + N_e P_{ee} \Delta c'\, r(v_e) + N_e P_{ee}^{coup} \Delta c'\, r(v_e')$$

$$\frac{dv_r}{dt} = -\frac{1}{\tau_r}v_r + \frac{f(u_r)}{A_r} + N_r P_{rr} J_{rr} r(v_r) + N_t P_{tr} J_{tr} r(v_t) + N_e P_{er} J_{er}\, r(v_e) + N_e P_{er} J_{er}' r(v_e')$$

$$\frac{du_r}{dt} = \left[\frac{1}{\tau_r^u}(b_r - u_r)\right]$$

$$\frac{dv_t}{dt} = -\frac{1}{\tau_t}v_t + \frac{f(u_t)}{A_t} + N_r P_{rt} J_{rt} r(v_r) + N_e P_{et} J_{et}\, r(v_e) + N_e P_{et} J_{et}'\, r(v_e')$$

$$\frac{du_t}{dt} = \left[\frac{1}{\tau_t^u}(b_t - u_t)\right]. \tag{9}$$

To solve the nonlinear dynamical system of the model we used a fourth-order Runge–Kutta method with a time step of 1 ms and run it within MATLAB R2015b.

2.3. Experimental protocol

We recruited 20 volunteers for this study. Participants were right-handed undergraduate/graduate students of Ferdowsi University of Mashhad (3 females; age range of 19–29 years with mean ± SEM of 21.8 ± 0.7 years). All subjects were with normal body mass index (21.5 ± 0.5 kg/m^2, mean ± SEM), had normal hearing, and had no history of any neurological disease. They reported normal nocturnal sleep patterns (7–9 h starting from 10 p.m. to 12 a.m.) for the week before the experiment. They had not used caffeine, nicotine, or energy drinks on the experiment day and had not performed excessive exercise in the 24 h before the experiment. Subjects were instructed to sleep 2 h less than their normal routine (at least 5 h) the night prior to the experiment and take no nap in the day before the experiment. Written informed consent was obtained from all subjects. The experimental protocols were approved by the Ethics Committee of the Ferdowsi University of Mashhad. All volunteers were rewarded with either monetary compensation or course credits.

All subjects attended an adaptation session a few days prior to the experiment which allowed them to become familiar with the experimental setup, procedures, and the EEG recording room, in which they were instructed to take a nap. On the experiment day, subjects arrived at the lab at ~10 a.m. They watched a movie until 12 p.m. and then engaged in a word-pair associate learning task. Later, they were allowed to rest and had lunch. At 2 p.m. they were prepared for EEG recording and were instructed to nap in the EEG recording room as long as they could but maximally for 1.5 h after the recording onset.

2.4. Sleep EEG recording and preprocessing

EEG Data were acquired using a g. USBamp (g.tec Medical Engineering GmbH, Austria) from 28 active electrodes located at F3, F1, Fz, F2, F4, FC5, FC3, FC1, FCz, FC2, FC4, FC6, C5, C3, C1, Cz, C2, C4, C6, CP5, CP3, CP1, CPz, CP2, CP4, CP6, P3, P4, according to the 10–20 system, with a sampling frequency of 512 Hz. Horizontal and vertical electrooculography (EOG) and chin electromyography (EMG) were monitored throughout the nap. A band pass 0.1–60 Hz filter was applied to remove low and HF artifacts from the EEG signals. A notch 50 Hz filter was used to remove the powerline noise. Movement artifacts were removed through visual inspection of the data. For reduction of artifacts corresponding to high frequencies, EEG data were excluded whenever within a 50 ms sliding window the STD of filtered EEG above 20 Hz exceeded a threshold determined by visual inspection for each subject. EEG electrodes FCz, Cz, and PCz along with EOGs and chin EMG were used for sleep staging. For each subject, 30 s epochs of sleep EEG were visually scored according to the AASM standard (Berry et al., 2012) into stages 1, 2, 3 and REM sleep, with stage 2 corresponding to light non-REM sleep, and stages 3 corresponding to SWS. Average timing of

stages during the afternoon nap for the subjects is given in Table S2. The first 22 min of SWS was used for further processing. Data from four subjects (out of 20 subjects) were discarded; one due to the high content of noise and three with SWS duration of less than 22 min. Some of the analyses were performed on an ROI consisting of the fronto-central electrodes FCz and Cz with pronounced spectral peaks in the frequency ranges of interest; slow oscillation (SO), 0.5–2 Hz, slow spindle and fast spindle, 8–12 Hz and 12–16 Hz, respectively as well as HF oscillations, 20–30 Hz (see Fig. S2 for the scalp map of power distribution over the aforementioned frequency ranges).

2.5. Slow oscillations and spindles detection

The algorithm employed for detecting slow oscillations from the results of the model was the same as what was previously employed by Klinzing et al. (2016) except for the threshold used during the identification phase. Briefly, the membrane potential was filtered into the bandwidth 0.5–2 Hz using FIR filters from the EEGLAB toolbox (Delorme and Makeig, 2004). Next, the negative peak of slow oscillations was determined if the amplitude of the negative peak was larger than 1.4 times the averaged negative peak.

Detection of spindles was the same in details for the EEG signals and the results of the model unless stated otherwise. For spindle detection a previously introduced approach (Klinzing et al., 2016) was employed. EEG signals corresponding to SWS were bandpass filtered with FIR filters between 8-12 Hz and 12–16 Hz for detecting slow and fast spindles, respectively, using FIR filters from the EEGLAB toolbox. For the results of the model, bandpass filters of bandwidth 4 Hz were centered at the peak frequency of slow and fast spindles corresponding to 8–12 Hz for slow spindles and 13–17 Hz for fast spindles. Next, the root mean square (RMS) of the filtered signals was calculated and smoothed using a moving average window of length 0.2 s. After computing the STD of the filtered signals a threshold was defined as 1.5 × STD (1 × STD for the results of the model). A spindle was detected if the RMS signal remained above the defined threshold for 0.5–3 s. Once the spindles were detected the time point of spindle event was defined as the time of maximum peak. The details of detected events for each subject are presented in Table S3. For slope calculation, in the signal filtered below 30 Hz, the spindles were averaged over a 4 s window centered at the event time point and smoothed using a 300 ms moving average. Next, the instantaneous slope was computed and averaged over ±150 ms.

2.6. Spectral analysis

Spectral power analysis was performed using fast Fourier transform (FFT) and a Hanning window of length 10 s with 50% overlap. For each subject, average power spectra corresponding to the first 22 min of SWS was calculated. We clustered the subjects based on their HF power (20–30 Hz); subjects were ranked based on their HF power and the fourth and fifth octiles (8-quantiles) were discarded, to create two clusters of subjects with relatively large and small HF power. Each cluster included six subjects. The power spectra of the two aforementioned clusters were then statistically compared over a moving window of length 4 Hz with 90% overlap.

We investigated the time-varying oscillatory brain activity by means of wavelet based time-frequency analysis (Klinzing et al., 2016; Tallon-Baudry et al., 1997). We used a complex Morlet wavelet with a Gaussian shape both in time and in frequency domains (Mallat, 1999). The value of η which determines the relationship between the center frequency and the bandwidth, $\eta = \frac{f}{\sigma_f}$, and also affects both the temporal and frequency resolutions was set to 12 based on the frequency range of interest. The power spectra at each time and frequency bin was then computed as the wavelet energy over frequency as well as time steps.

The HF (20–30 Hz) power content was investigated ±1 s around the slow and fast spindle events. The mean power around the slow/fast spindle event, $P^{event}_{slow/fast}(t,f)$, was calculated for each subject. Moreover, for each subject 200 fragments of length 2 s were randomly selected from SWS. The mean power over time as well as fragments was then calculated and noted as $P^{non-event}_{slow/fast}(f)$. We made sure that the non-event fragments did not include any of the corresponding slow/fast spindle events. The normalized event related power corresponding to each subject was then calculated as $\overline{P}^{event}_{slow/fast}(t,f) = \frac{P^{event}_{slow/fast}(t,f) - P^{non-event}_{slow/fast}(f)}{P^{non-event}_{slow/fast}(f)}$. The same method is used to find the HF power content around spindles for the result of the model.

To find the peak frequency of each spindle event, first the spindle events were detected with the same method explained above by using a broad frequency range of 8–16 Hz. Next the spectrum in an interval of 10s around the spindle event was computed using 95% overlapping windows of 1.5 s and the frequency corresponding to the maximum power was identified with a frequency resolution of 0.5 Hz.

2.7. Statistical analysis

Wilcoxon signed-rank tests were used for model data which were not normally distributed. Student's t-tests were used for experimental data which were normally distributed. We checked whether the data were normally distributed using the Lilliefors modification of the Kolmogorov-Smirnov test ($P > 0.05$). Differences in the HF power before fast and slow spindle event were tested by mean of Mann-Whitney U— tests. The Friedman tests followed by Dunn-Sidak post hoc tests were used to investigate the difference between control, 25 Hz STIM and 35 Hz STIM conditions. The relationship between slow/fast spindle power/frequency and HF power were investigated via Pearson's correlation.

MATLAB was used for all statistical analysis. The data and code will be available from the corresponding author on request.

3. Results

3.1. Oscillations with the fast spindle frequency in the isolated thalamus

The interaction between RE and TC neurons in the isolated thalamus generates self-sustained oscillations only in the fast spindle frequency range (Fig. 1, by varying the synaptic strength the network produces oscillations only in the range of 14–20 Hz). Two identical groups of TC neurons (TC and TC') with different initial conditions are assumed which burst once every two cycles in agreement with the experimental observations (Kim et al., 1995). The thalamic model and the mechanism of oscillations in the fast spindle frequency range is similar to the one explained in a previous paper (Destexhe, 2009). In brief, the hyperpolarization of TC neurons caused by the inhibitory input form the RE neurons in one cycle, produces bursting activity of TC neurons in the next cycle. The excitatory post-synaptic potential (EPSP) from TC neurons in turn results in the firing of RE neurons in the next cycle. The inhibitory post-synaptic potential (IPSP) from the RE neurons and the inactivation of bursting variable reduce the membrane potential of TC neurons toward the resting potential which is followed by the decrease in the membrane potential of RE neurons. The IPSP from RE neurons also hyperpolarizes TC' neurons resulting in bursting of these neurons in the next cycle and the activity of neurons repeats again.

3.2. Cortical high frequency activity during up state

As we explained in a recent paper (Ghorbani et al., 2012), isolated cortex consisting of uniform networks of coupled excitatory and inhibitory neurons with excitatory-excitatory synapses subject to DSFA generates up and down states. An important problem with the uniform network is that the produced up state activity is much more regular than the experimentally observed noisy up-state. As we explained in a recent paper (Ghorbani et al., 2012), this problem is resolved by considering two weakly-coupled networks of excitatory and inhibitory neurons

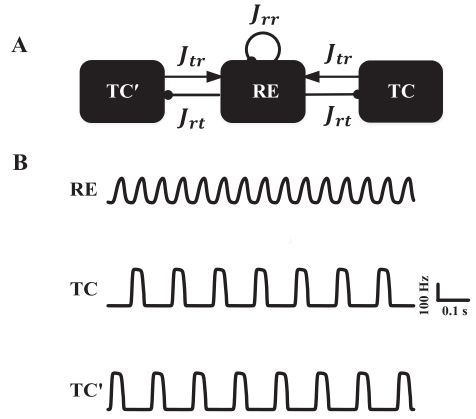

Fig. 1. Thalamus generates oscillations in the spindle frequency range. (A) Thalamus consists of two identical groups of thalamocortical neurons (TC, TC') and one group representing thalamic reticular neurons (RE). Excitatory synaptic connections are shown by arrows while inhibitory connections are indicated as lines ending in a dot. (B) Self-sustained oscillations in the fast spindle frequency range are generated in the thalamus. RE neurons fire at spindle frequency while TC neurons fire once every two cycles.

(network 1 and network 2) representing two regions of the cortex. This simple deterministic model produces UDS with stochastic high-frequency up-state activity due to partial synchronization of two UDS oscillators (Ghorbani et al., 2012). While the two cortical networks undergo synchronized transition between the two states they show uncorrelated HF fluctuations during the up state. This partial synchronization takes place when the strength of excitatory coupling between the two cortical networks is one order of magnitude less than the strength of the excitatory coupling between the excitatory neurons of each network resembling a small world network. The HF activity during the up state of the uniform network depends on the strength of the synaptic connections as is obtained in Eq. (8). Especially during the up state, progressively increase in the adaptation parameter, c, due to DSFA, reduces the strength of excitatory-excitatory connections which in turn decreases the frequency of oscillations (Fig. 2A). The oscillation frequency during the up state is also a decreasing function of the strength of inhibitory-inhibitory connection in the non-uniform model (Fig. 2B). As we later want to investigate the role of HF activity, the synaptic strength between the inhibitory neurons of network 1 is around half of the one of network 2 (Table S1) so that the neurons of network 1 show more HF activity compared to neurons of network 2.

3.3. *Fast spindle activity during UDS in the thalamocortical network as a result of bursting activity of thalamocortical neurons*

In the full model the two UDS cortical oscillators are coupled to the thalamic oscillators consisting of one group of identical TC neurons and one group of identical RE neurons (see Methods, Fig. 3A. For simplicity here we consider only one group of TC neurons). As explained above, bursting activity of TC neurons which is controlled by the bursting parameter b (defined in Eq. (2)), is essential for the generation of fast spindles. Bursting parameters were chosen to obtain results similar to the experimentally observed response of the TC and RE neurons to depolarizing and hyperpolarizing input currents in both tonic and burst modes (Fig. S1) and b was set to be −200 mA. However, to investigate the effect of bursting, we progressively increased the bursting ability of TC neurons by changing the bursting parameter b, from zero to −300 mA. We next calculated and analyzed the power spectrum of only cortical excitatory neurons of network 1 and network 2 (EX and EX' respectively) which is more comparable with scalp-recorded EEG (Buzsáki et al., 2012; Sotero and Trujillo-Barreto, 2008) (Fig. 3B). At b = 0 the thalamic input to the cortex was very small and hence the cortical power spectrum was similar to the isolated cortex with a broad peak at HF range. As the absolute value of b increased (b is a nonpositive parameter) a distinct peak at fast spindle frequency range appeared in both cortical groups. Further increasing of |b| resulted in the emergence of another peak at slow spindle frequency range only in the power spectrum of neurons of network 1 which is the network with higher HF activity. At larger values of |b|, the peak at fast spindle frequency range increased while the peak at slow spindle frequency range diminished. The changes in the mean power of both fast and slow spindles (13–17 Hz and 8–12 Hz respectively) as a function of b value is shown in Fig. 3B. While reducing the bursting activity of thalamic neurons from b = −200 mA to zero reduced the fast spindle power considerably (from $1.6 \pm 0.0204\ mV^2$, mean ± SEM at b = −200 mA to $0.85 \pm 0.0116\ mV^2$ at b = 0), slow spindle power remained less affected (from $1.30 \pm 0.0152\ mV^2$, mean ± SEM at b = −200 mA to $1.44 \pm 0.0183\ mV^2$, mean ± SEM at b = 0). This result is in a good agreement with a recent study showing differential effect of reducing the efficacy of Ca^{2+} channels for slow and fast spindles (Ayoub et al., 2013).

At around b = −200 mA, EX neurons show two distinct peaks at both slow and fast spindle frequency ranges (Fig. 3C) and the thalamocortical network reproduces oscillations similar to up and down states during slow wave sleep as well as spindle activity (Fig. 3D). Due to nonlinear interaction of multiple weakly coupled oscillators, the oscillations are highly irregular with stochastic duration of up state and spindle activity. The power spectrum of the two cortical groups has a distinct peak at fast spindle frequency range (peak frequency = 15 Hz). The fast spindles are generated within the thalamus but the beginning and termination of them are controlled by the excitatory cortical input. When RE neurons start to fire as a result of the down to up transition of cortical neurons, the inhibitory input from the RE neurons which is dominant to the cortical excitatory input produces hyperpolarization in TC neurons. The bursting parameter decreases from zero to its new negative equilibrium value as a result of this hyperpolarization which leads to bursting activity of TC neurons. Next the interaction between TC and RE neurons produces oscillations with the fast spindle frequency. On the other hand, due to

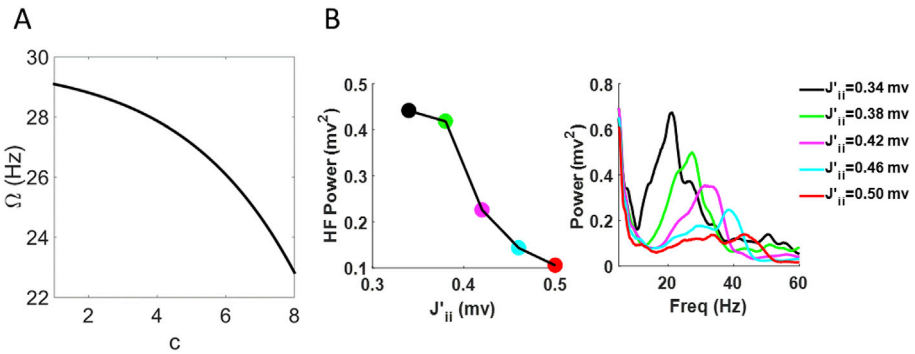

Fig. 2. HF oscillations of the isolated cortical network. (A) The oscillation frequency during the up state as a function of the adaptation variable, c, for a uniform network consisting of one excitatory and one inhibitory neuron, obtained from Eq. (8) with parameters of cortical network 1 (Table S1). (B) The power spectrum of the excitatory neuron of network 2 for different values of the strength of inhibitory-inhibitory connections in the non-uniform model (Right). HF power (20–30 Hz) as a function of the strength of inhibitory-inhibitory connections (Left).

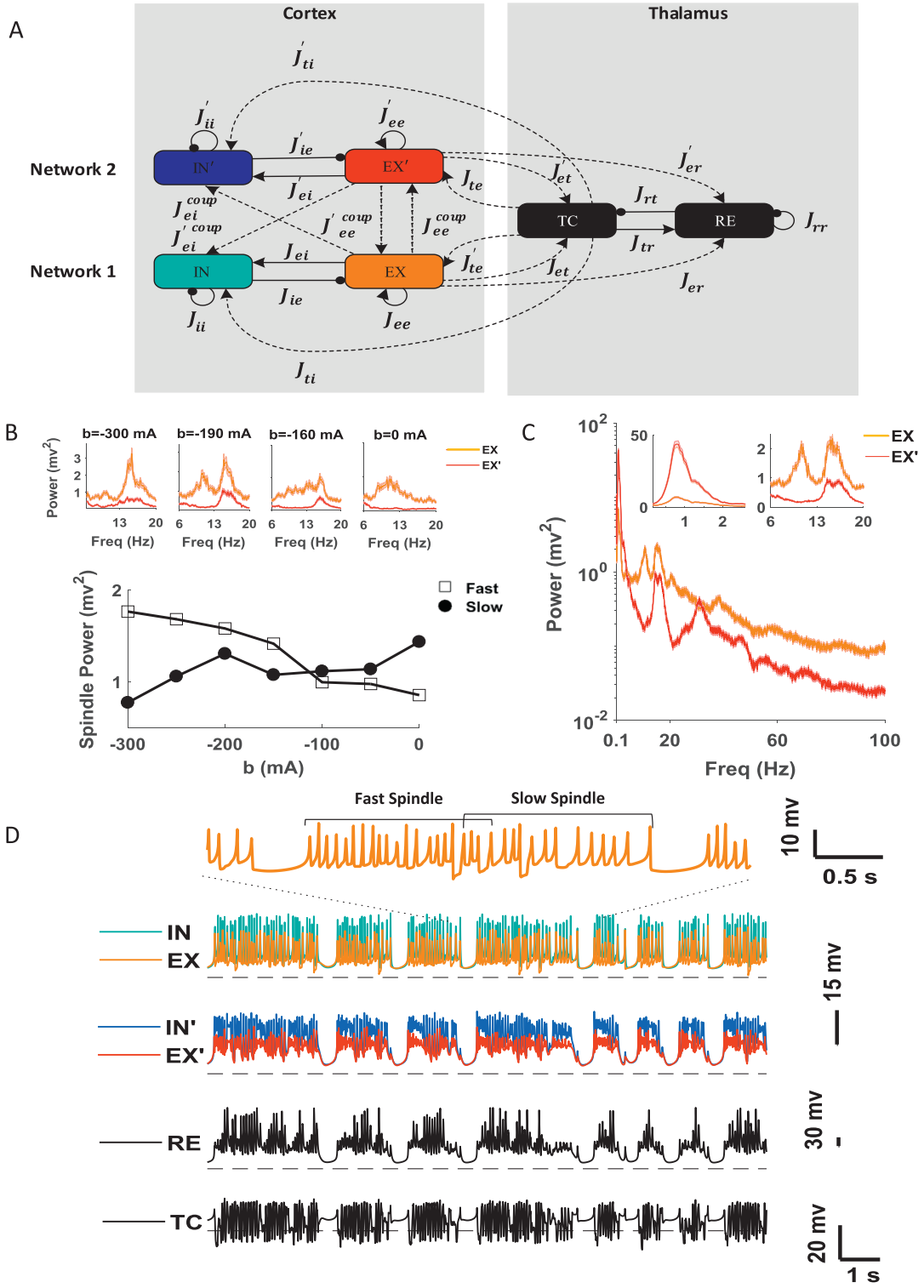

Fig. 3. Slow and fast spindles during up and down states in the thalamocortical network. (A) Tow cortical networks (Left) and thalamus network (Right) are recurrently connected in the full thalamocortical model. Thalamus network consists of one group of identical TC neurons and one group of identical RE neurons. Each cortical network consists of one group of identical excitatory (EX) neurons and one group of identical inhibitory (IN) neurons. The variables and parameters of network 2 are shown by primes. Different networks are connected only by long-range excitatory synapses (dotted lines). (B) Power spectrum of EX and EX' neurons (orange and red respectively) for four different values of bursting parameter, b (Top). Mean power of EX neurons at slow and fast spindle frequency range (8–12 Hz, filled circles, and 13–17 Hz, empty squares, respectively) as a function of bursting parameter, b (Down). (C) Power spectrum of cortical excitatory neurons at b = −200 mA. The peak of slow spindle appears only in the power spectrum of network 1 with larger amplitude at HF (orange). (D) Self-sustained oscillations including UDS, slow and fast spindles are reproduced in the thalamocortical network. The amplitude of HF oscillations is higher in network 1 (orange and cyan curves corresponding to membrane potential of EX and IN) compared to network 2 (red and blue curves corresponding to the membrane potential of EX' and IN'). Slow spindles are generated only in network 1 mostly at the end of the up states. The line shows the resting potential which is set to zero.

DSFA, the synaptic activity in the up state progressively reduces the ability of cortical excitatory neurons to respond to depolarizing synaptic inputs. Hence the activity of cortical excitatory neurons and so the RE neurons decrease towards the end of the up state which finally results in the termination of the fast spindle. The average membrane potential of TC neurons locked to the maximum peak of the fast spindle activity detected in EX neurons indicates synchronous spindle activity with slight but significant shift towards the negative time (-7 ± 0.1 ms, mean ± SEM, $p < 0.000001$, Wilcoxon signed-rank test) which is expected because of the thalamic origin of fast spindles (Fig. 4A).

3.4. Generation of slow spindles as a result of interplay between cortex and thalamus

We hypothesized that the superposition of thalamic fast spindles and cortical HF activity could produce slow spindles in the full thalamocortical network. In addition to the fast spindle, the power spectrum of the neurons in network 1 has a distinct peak at slow spindle frequency range (peak frequency = 10.6 Hz, Fig. 3C). This peak in the slow spindle frequency range is absent in the power spectrum of neurons in network 2 which has less HF power compared to network 1. Moreover, while the power spectrum of network 1 at HF is larger than the one of network 2, the peak in the power spectrum at low frequencies (~1 Hz) corresponding to SO activity, is larger in network 2 compared to network 1. The average membrane potential of TC neurons locked to the maximum peak of the slow spindle activity detected in EX neurons indicates synchronous slow spindle activity (Fig. 4A). However, it seems that the oscillation frequency of TC neurons is larger than the oscillation frequency of EX neurons during the slow spindle. To show this behavior more clearly, we next calculated the average wavelet-power of TC neurons during slow spindle detected in EX neurons (± 1 s) around its maximum peak (Fig. 4B) which indicated that while EX neurons oscillated dominantly at slow spindle frequency range, TC neurons oscillated with dominant frequency in the range of fast spindles.

3.5. Distinct coupling of slow and fast spindles with SO and HF oscillations

We assume that the interaction between HF oscillations of network 1 and the excitatory input from the thalamus produces the slow spindles. In order to further investigate the association between HF oscillations and slow spindles, the average wavelet-power of EX neurons during both slow and fast spindles (± 1 s) around their maximum peak were plotted (Fig. 4B). We found that only for slow spindles, HF power significantly ($p < 0.001$, Wilcoxon signed-rank test, compared to non-event, see Methods) increased before the maximum peak of spindle event (there is another increase in power around zero time for both slow and fast spindles which occurred at frequencies corresponding to harmonic of slow and fast spindle frequencies respectively). Moreover, by comparing the averaged HF power in a 1 s interval before the spindle event we found that HF activity was significantly larger before the slow spindle compared to the fast spindle (Fig. 4 C, $p < 0.001$, Mann-Whitney U— test, 35.2 ± 0.03 dB, mean ± SEM for slow spindle and 34.1 ± 0.04 dB for fast spindle).

During the up state, as a result of increasing the c value due to DSFA, the frequency of cortical HF oscillations decreases towards the end of the up state (Fig. 2 A). Hence while fast spindles occurred mostly in the beginning of the up state, slow spindles were mainly produced towards the end of the up state (Fig. 3D). This trend was also observed in the

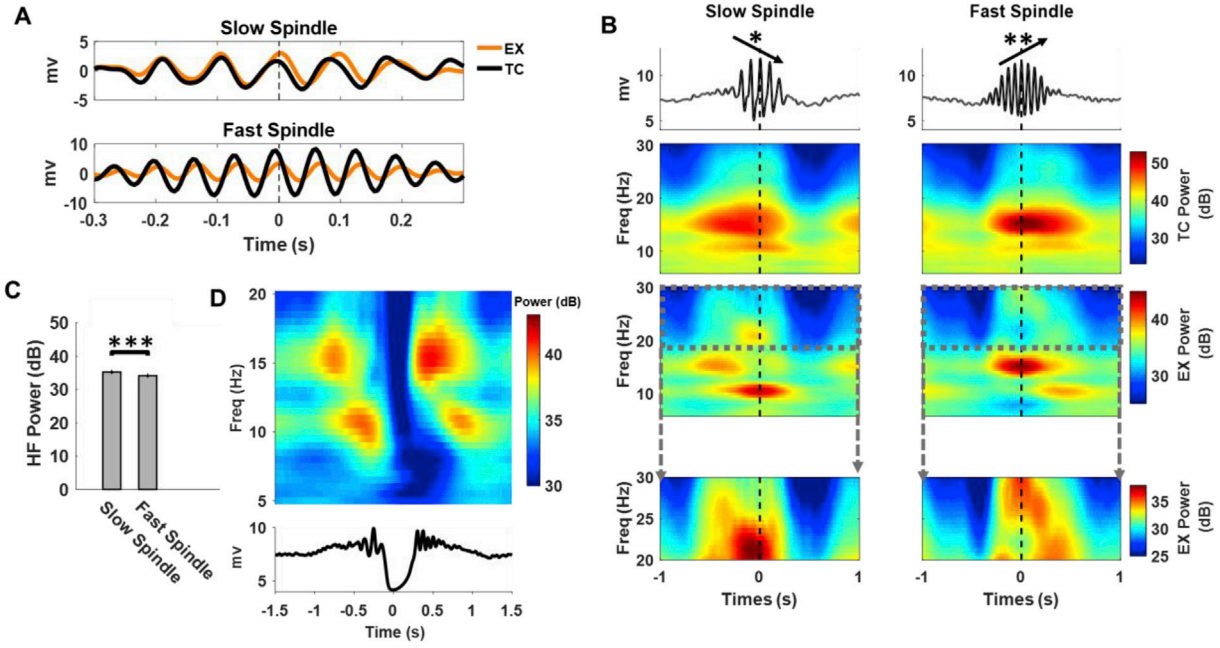

Fig. 4. Distinct properties of fast and slow spindles. (A) Average activity of TC neurons (black) locked to the time of the maximum peak of slow spindles detected in EX neurons, n = 2858. The average slow spindle activity of Ex neurons is shown in orange (Top). Average activity of TC neurons (black) locked to the time of the maximum peak of fast spindles detected in EX neurons, n = 2867. The average fast spindle activity of Ex neurons is shown in orange (Bottom). (B) Averages of the membrane potential of EX neuron across all detected slow (Left, n = 2867) and fast (Right, n = 2858) spindles (Top). Averaging was performed with reference to the maximum peak of the detected slow and fast spindles. Asterisks (and arrows) show a significant (*$p < 0.05$, ***$p < 0.000001$) negative and positive slope of fast and slow spindles, respectively, in the interval between 150 ms before to 150 ms after the spindle. Wavelet power of the membrane potential of TC (Middle) and EX (Bottom) neurons during slow (Left) and fast (Right) spindles with reference to the maximum peak of the detected spindles in EX neurons, averaged over all spindles. To show the distinct coupling of slow and fast spindles with HF activity more clearly, HF wavelet power for frequencies 20–30 Hz is shown separately. (C) Averaged HF power in a window of 1 s before the event of slow and fast spindles. (D) Time-frequency representation of average wavelet power of the membrane potential of cortical excitatory neuron of group 1, EX, during a time window of ±1.5 s around the negative peak of down state for frequencies 5–20 Hz (Top, n = 3767). Average of the membrane potential of EX neuron filtered below 30 Hz over all detected slow oscillations in a time window of ±1.5 s around the negative peak of slow oscillations (Bottom).

average signal time-locked to fast as well as slow spindles (using the maximum peak of the filtered data, Fig. 4B). On averaged slow spindles were on top of a downward background signal with significant negative slope (-0.32 ± 0.06 mV/s, mean ± SEM, $p = 0.02$, Wilcoxon signed-rank test) while the background signal during the fast spindles increased around zero time showing a significant positive slope (0.55 ± 0.05 mV/s, mean ± SEM, $p < 0.000001$, Wilcoxon signed-rank test). To show this coupling more clearly the average wavelet-power around the trough of down state (± 1.5 s) was plotted for the excitatory neurons of cortical network 1 (Fig. 4D). In a very good agreement with the previous experimental observations, the slow spindle power strongly increased at the end of the up state while fast spindle power was stronger in the beginning of the up state. Both fast and slow spindle powers suppressed during the down state and only for the slow spindle the suppression remained after the transition to the up state. This further confirms the temporal relationship between UDS and spindles that has been reported experimentally.

3.6. The dependence of the slow spindle peak on cortical parameters

In order to further show the distinct mechanism of slow and fast spindles we investigated the changes of two peaks corresponding to fast and slow spindles in the power spectrum of the excitatory neurons of network 1 by varying three cortical parameters. We found that the increase of the adaptation parameter, Δc (from 3.4 to 5.5 $\times 10^{-3}$, see Methods), changed the frequency of the peak corresponding to slow spindle towards lower frequencies while had a minor effect on the frequency of fast spindle (from 11.5 to 9.5 for slow spindle and from 15.2 to 15.5 Hz for fast spindle, Fig. 5A). The increase in Δc also decreased the HF activity defined as the mean power between 20 and 30 Hz (from 0.75 to 0.48 mV^2, Fig. 5B). We next calculated the changes in slow spindle power (from 2.1 to 1.42 mV^2, Fig. 5B) as a function of HF activity caused by varying Δc (Fig. 5B). In agreement with our hypothesis, the power at slow spindle range was positively correlated with HF activity. Next, to investigate the effect of cortical excitatory to excitatory connections, we multiplied the strength of all of these connections (both short and long range) by a constant, k (changing from 0.86 to 1.06), and found that the HF power as well as the slow spindle power increased by increasing the strength of cortical excitatory to excitatory connections (from 0.3 to 1.7 mV^2 for slow spindle and from 0.14 to 0.7 mV^2 for HF power, Fig. 5C). There is also a positive correlation between fast spindle power and HF power (Fig. 5B and C). In addition, the increase of the excitatory input from network 2 to excitatory neurons of network 1, $J_{ee}^{'coup}$ (from 0.35 to 0.51 mV), enhanced the peak amplitude of fast spindle (from 1.9 to 2.6 mV^2) while it reduced the peak amplitude of slow spindle (from 1.71 to 1.5 mV^2) and finally at large value of $J_{ee}^{'coup}$, the peak of slow spindle disappeared (Fig. 5D). These results further support the distinct mechanism for the generation of slow and fast spindles and show that unlike the fast spindle peak, the presence of slow spindle peak depends on the cortical parameters.

3.7. Slow to fast spindle transition as a result of increasing the strength of cortico-thalamic connections

We next studied the changes in the slow and fast spindle activity by varying the strength of the connection between cortical excitatory neurons and TC neurons (Fig. 6). We hypostatized that the changes in the strength of this cortico-thalamic connection might explain the differences in the relative slow and fast spindle activity at different cortical regions especially from frontal to parietal lob. For low values of $J_{et}^{'}$ the power spectrum of EX neurons has a dominant peak at slow spindle frequency range with no considerable peak at fast spindle frequency range (condition 1). Interestingly for the same value of $J_{et}^{'}$, power spectrum of TC neurons and the excitatory neurons of the cortical network with less HF activity (EX') only have a peak at fast spindle frequency range. By increasing $J_{et}^{'}$ the power of EX neurons at HF and slow spindle frequency ranges increases (Fig. 6B). At $J_{et}^{'} \sim 1.5$ mV a transition occurs so that the dominant peak in the power spectrum of EX neurons shifts from slow spindle to fast spindle frequency range. Around this threshold value both slow and fast spindle activity are considerable (condition 2). Further increasing of $J_{et}^{'}$ increases the power at fast spindle frequency range while decreases the power at slow spindle frequency range as well as HF power (condition 3). Finally at larger values of $J_{et}^{'}$ only the fast spindle peak remains and the slow spindle peak disappears (condition 4). It is important to mention that this slow to fast spindle transition is absent in the power spectrum of TC and EX' neurons so that always their power spectrum only has a peak at fast spindle frequency range. This slow to fast spindle transition is similar to the previously reported (Andrillon et al., 2011; Mölle et al., 2011) changes in the relative slow and fast spindle activity from frontal to parietal lobe suggesting that conditions 1, 2, 3 and 4 might correspond to frontal, frontocentral, central, centroparietal/parietal lobes respectively.

3.8. Emergence of slow spindles by HF stimulation

To directly investigate the causal role of HF oscillations on slow spindle activity, we next studied the effect of HF stimulation on the result of the model. We hypothesized that applying external stimulation with dominant frequency of $f_2 \sim 25$ Hz to cortical neurons could interact with the thalamic input at fast spindle frequency range ($f_1 \sim 13 - 17$ Hz) and result in the oscillations with frequency in the range of the difference between the two frequencies of the two inputs ($f_2 - f_1 \sim 8 - 12$ *Hz*) that lies in the frequency range of slow spindles. The external stimulation was pink 1/f noise with a frequency range of 25–35 Hz (25 Hz STIM) applied only to the excitatory neuron of network 2 (EX'), i.e. the network with less HF activity. Whenever a slow spindle was detected only in the excitatory neuron of network 1 (no slow spindle was detected in the excitatory neuron of network 2 in a duration of 1 s before and after the onset of slow spindle of EX neurons), the stimulation was applied for a duration of 400 ms from 200 ms before the onset of the detected slow spindle of EX neurons (Fig. 7A). This HF stimulation significantly increased the slow spindle power (averaged over 800 ms window after the onset of stimulation, from 0.0095 ± 0.005 mV^2, mean ± SEM corresponding to Control condition to 0.05 ± 0.0014 mV^2, $p = 0.002$, Wilcoxon signed-rank test) and so enhanced the probability of slow spindle occurrence (Fig. 7B). Moreover, slow spindle power increased as the amplitude of stimulation enhanced (Fig. 7C). We next investigated the effect of stimulation frequency by applying another stimulation with a dominant frequency of 35 Hz (1/f noise with a frequency range of 35–45 Hz with the same amplitude of 25 Hz STIM). We found a significant difference among the three groups (Fig. 7D, Friedman test, Chi-sq = 15.2, $p < 0.001$). While 25 Hz STIM significantly increased slow spindle power ($p = 0.02$, Friedman test with Dunn-Sidak *post hoc* test), 35 Hz STIM did not change the slow spindle power significantly (0.01 ± 0.0011 mV^2, mean ± SEM, $p = 0.65$, Friedman test with Dunn-Sidak *post hoc* test). Moreover, comparing the effect of 35 Hz STIM with 25 Hz STIM, we found that slow spindle power was significantly larger for 25 Hz STIM ($p = 0.0005$, Friedman test with Dunn-Sidak *post hoc* test, Fig. 7D). These results are in a very good agreement with our proposed mechanism since the difference between fast spindle frequency range and a dominant frequency of 35 Hz corresponding to the second stimulation lies out of the frequency range of slow spindle.

3.9. The relationship between HF oscillations and slow sleep spindles in human EEG

We have shown that this simple model is able to capture the experimentally observed different modulation of slow and fast spindles with UDS. Moreover, this model predicts that slow spindles are associated with cortical HF oscillations. To check this prediction experimentally, we

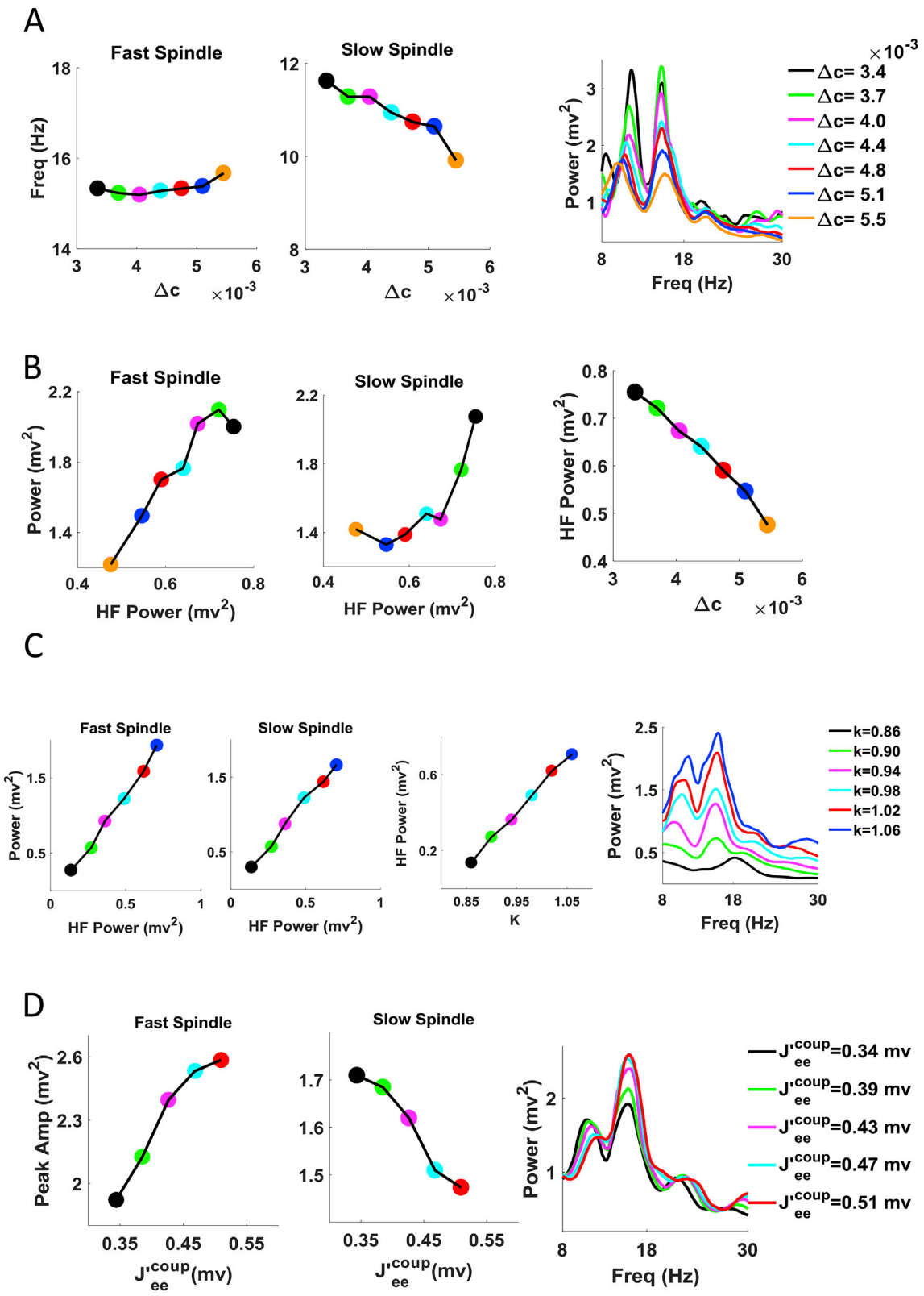

Fig. 5. The dependence of slow spindle peak on cortical parameters. (A) Changes in the power spectrum of EX neurons as a result of the variation of the adaptation parameter, Δc (Right). The spindle peak frequency versus Δc is plotted for slow (Middle) and fast (Left) spindles. (B) HF (20–30 Hz) power versus Δc (Right). Changes in the slow (Middle) and fast (Left) spindle power (8–12 Hz and 13–17 respectively) versus changes in HF power as a result of the variation of Δc. (C) Changes in the power spectrum of EX neurons as a result of the variation of all (both short and long range) cortical excitatory to excitatory connections by multiplying a constant, k. k = 1 corresponds to the values of the parameters shown in Table S1 (Right). HF (20–30 Hz) power versus k (Middle). Changes in slow and fast spindle power versus changes in HF power as a result of the variation of k (Left) (D) Changes in the power spectrum of EX neurons as a result of the variation of long range excitatory connection from EX' to EX, J'^{coup}_{ee} (Right). The spindle peak amplitude versus J'^{coup}_{ee} is plotted for slow (Middle) and fast (Left) spindles.

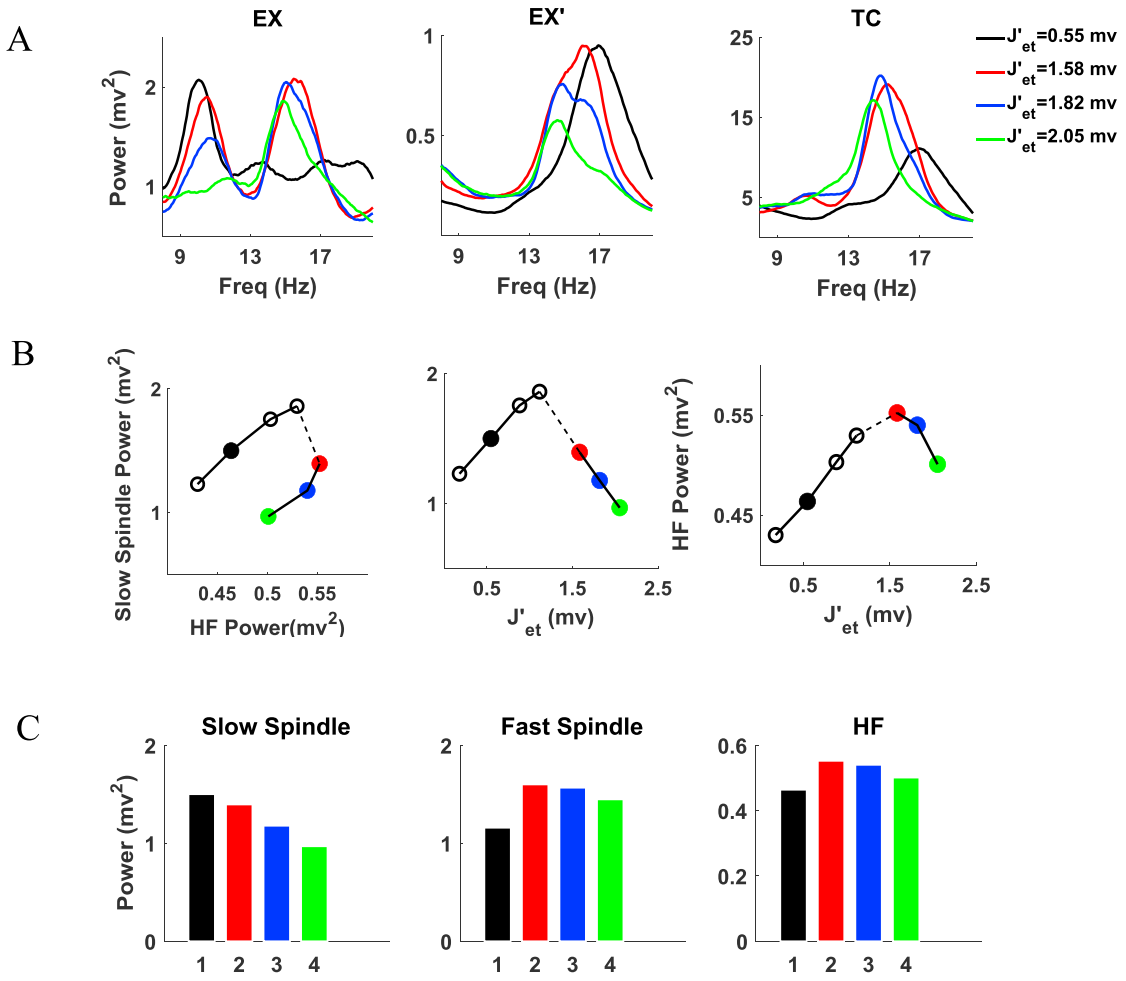

Fig. 6. Slow to fast spindle transition by increasing the strength of the connection from cortical excitatory neurons to thalamocortical neurons (J'_{et}). (A) The power spectrum of EX (Left), EX' (Middle) and TC neurons (Right) for four conditions corresponding to different values of J'_{et}. The power spectrum corresponding to the empty circles in not shown. (B) Slow spindle power versus HF power for different values of J'_{et} (Left). Slow spindle power (Middle) and HF power (Right) versus J'_{et}. (C) Slow spindle (Left), fast spindle (Middle) and HF (Right) power compared between four conditions (1, 2, 3, 4 corresponds to $J'_{et} = 0.55$, 1.58, 1.82 and 2.05 mV respectively).

recorded EEG from subjects during nap (see Methods). We first calculated the power at slow (8–12 Hz) and fast (12–16 Hz) spindle frequency bands and plotted them versus HF (20–30 Hz) power for all subjects (Fig. 8A, analyses were performed on an ROI consisting of the fronto-central electrodes FCz and Cz with pronounced spectral peaks in the frequency ranges of interest, see Fig. S2). In agreement with the model result (Fig. 5B and C), there was a significant positive correlation between HF power and both slow and fast spindles (Pearson's correlation coefficient $r = 0.7$, $p = 0.003$ for slow spindle and $r = 0.7$, $p = 0.001$ for fast spindles). We then grouped the subjects into two groups of subjects with relatively high and low HF power (Fig. 8B) and compared the spectral content of each group at other frequencies (Fig. 8C). The slow and fast spindle frequency powers were significantly larger for the group with more HF power (for slow spindle frequency, $p = 0.043$, unpaired *t*-test; $7.3 \pm 1.24\ \mu V^2$ mean ± SEM for low HF group and $12.94 \pm 2.1\ mV^2$ for high HF group; for fast spindle $p = 0.026$, Mann-Whitney U— test, $6.33 \pm 0.84\ \mu V^2$ mean ± SEM for low HF group and $11.53 \pm 2.46\ mV^2$ for high HF group). Topographies of slow spindle density and duration showed that their values were higher in high HF power group especially over frontal electrodes (Fig. S3). These results are in a very good agreement with the results of the model (Fig. 3C).

Moreover, calculating the average signal time-locked to spindles, we found that, on average slow spindles were on top of a downward background signal with significant negative slope ($-55 \pm 13.6\ \mu V/s$, mean ± SEM, $p = 0.001$, Wilcoxon signed-rank test, this slope was not significantly different from zero for fast spindles, $p = 0.1$, paired *t*-test). To investigate the temporal relationship between sleep spindles and HF oscillations, the same as model, we calculated the HF power content ±1 s around the maximum peak of slow and fast spindles. In agreement with the prediction of the model, HF power significantly increased before the maximum peak of slow spindles (Fig. 8D, $p < 0.05$, paired *t*-test, compared to non-event, see Methods, there is another increase in power around zero time for both slow and fast spindles which occurred at frequencies corresponding to harmonic of slow and fast spindle frequencies respectively). Moreover, by comparing the averaged HF power in a 1 s interval before the spindle event we found that similar to model prediction (Fig. 4 C) HF activity was significantly larger before the slow spindle compared to the fast spindle (Fig. 8 E, $p < 0.001$, paired *t*-test, 45.1 ± 0.5 dB, mean ± SEM for slow spindle and 41.6 ± 0.4 dB for fast spindle). This temporal correlation between slow spindles and HF power is supportive of the essential role of cortical HF activity in the generation of slow spindles.

To investigate more directly the association between HF power and the frequency of spindles, we detected all the spindles in a broad frequency range of 8–16 Hz and computed the frequency of each spindle event. Interestingly, we found a significant negative correlation between spindle frequency and HF power in a 1 s interval before the spindle event (Fig. 8 F, $r = -0.6$, $p = 0.03$, Pearson's correlation).

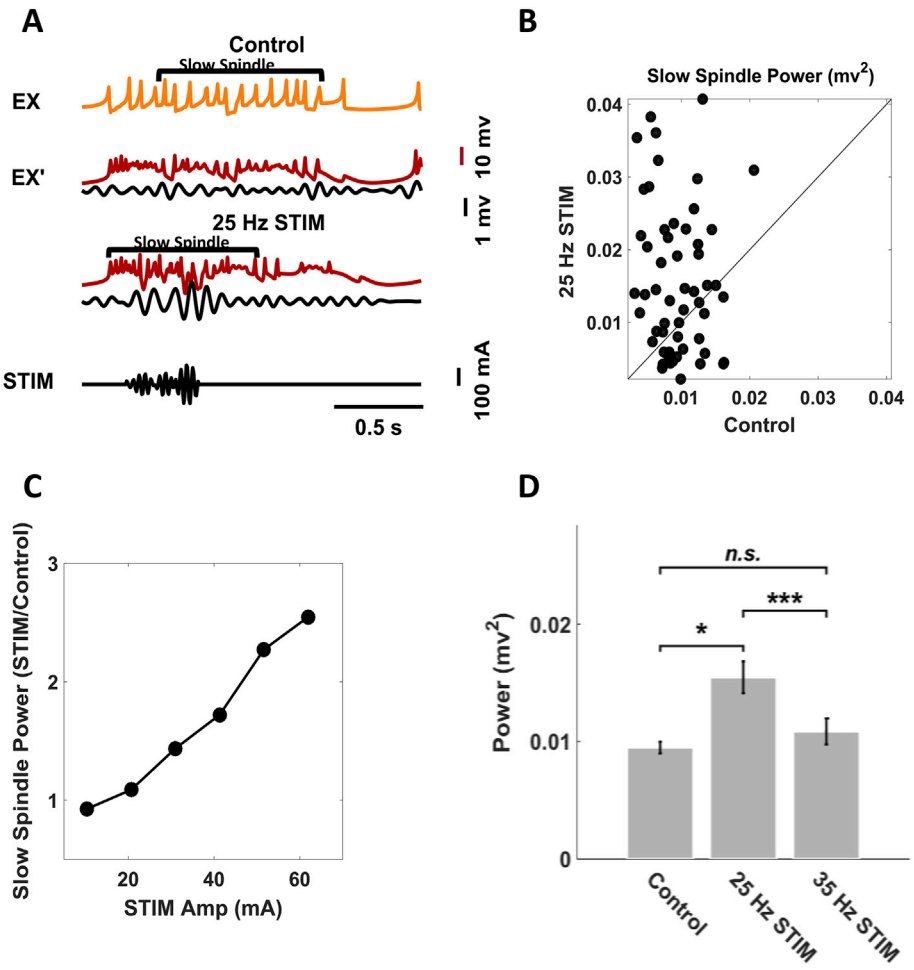

Fig. 7. The changes in the slow spindle activity of EX' neurons as a result of HF stimulation (A) Whenever a slow spindle was detected only in excitatory neuron of network 1, EX, (no slow spindle was detected in the excitatory neuron of network 2, EX', in a duration of 1 s before and after the onset of slow spindle of EX), the stimulation was applied for a duration of 400 ms from 200 ms before the onset of the detected slow spindle of EX. Membrane potential of EX (orange) and EX' (red) neurons for a time when without any stimulation (control), the slow spindle was generated only in EX neurons and not in EX' neurons. The membrane potential of EX' neuron filtered in the range of slow spindle is shown in black (Top). Membrane potential of EX' neuron after applying stimulation (Middle). Stimulation is a 1/f noise with a frequency range of 25–35 Hz (25 Hz STIM) and amplitude (root mean square) of 35 mA (Bottom). (B) Mean slow spindle power with 25 Hz stimulation versus the one without the stimulation ($p = 0.002$, Wilcoxon signed-rank test). The power was calculated over 800 ms window after the onset of stimulation and shown for 56 trials (C) Mean slow spindle power with 25 Hz stimulation averaged over 56 trials divided by the mean slow spindle power without stimulation as a function of the amplitude of the stimulation. (D) Slow spindle power for control, 25 Hz STIM and 35 Hz STIM (1/f noise with a frequency range of 35–45 Hz) conditions. The amplitude of the two stimulations is the same as A and B (*$p < 0.05$, ***$p < 0.001$, Friedman test with Dunn-Sidak *post hoc* test). Error bars represent standard error of the mean.

We next investigated the differences in the slow spindle, fast spindle and HF powers between frontal, frontocentral, central and centroparietal electrodes corresponding to Fz, FCz, Cz and CPz respectively. In agreement with the previous studies and model predictions, the slow spindle power was larger over Fz and FCz electrodes while fast spindle power was more centrally distributed (Fig. 9, Fig. S2). Moreover, the changes in the HF power from frontal to parietal regions was in a very good agreement with the model prediction by increasing the connection from cortical excitatory neurons to TC neurons (Fig. 6C).

4. Disscusion

While growing evidences indicate different features for slow and fast spindles during SWS, previous models of spindle generation are not able to explain these results. In addition to distinctive differences in frequency and topological distribution, recent studies (Klinzing et al., 2016; Mölle et al., 2011) reported that slow and fast spindles occur at opposing phases of the slow oscillations so that only fast spindles are dominant during down to up transition. The occurrence of slow spindles during up to down transition challenges the classical hypothesis that the transition to the up states facilitates the emergence of spindles. Moreover recently Ayoub et al. (2013) showed that reduction of Na^+ channel efficacy had an opposite effect on slow and fast spindles. Using Ca^{2+} antagonist they also found reduction in the fast spindle while slow spindle remained unaffected which raise a question relative to the hypothesis that low-threshold Ca^{2+} -dependent spike burst (LTS) is essential for spindle generation.

Overall, these findings suggest distinct mechanism for slow and fast spindles and a possible role of cortex in initiating of slow spindles. This simple thalamocortical model we propose here, spontaneously reproduces UDS as well as both fast and slow spindles. Due to DSFA, the frequency of cortical oscillations reduces during the up state. This results in higher slow spindle power at the end of the up state while fast spindles occur mostly in the beginning of the up state which is in a very good agreement with the previous experimental observations. In consistent with the Ayoub et al. experimental observations (Ayoub et al., 2013) we also showed that reducing the ability of TC neurons to burst largely decreased the fast spindle activity while the slow spindle activity remained less affected. In this model the oscillations in the fast spindle frequency range are produced in the thalamus but the beginning and end of spindles are controlled by cortical input to the thalamus. Moreover, the nonlinear interaction between thalamic oscillators at fast spindle frequency and cortical HF oscillators produces the slow spindles. To investigate the causal role of cortical HF activity on the generation of slow spindles we applied external HF input to the cortical group with lower HF activity and found a significant increase in the slow spindle activity of this group. Moreover, the average wavelet-power of cortical neurons during slow spindle revealed that HF activity increased before the maximum peak of slow spindle. This prediction of the model was further confirmed by recording and analyzing EEG from subjects during nap. We also divided the subjects into two groups of low HF activity and high HF activity and supportive to our hypothesis we found that slow and fast spindle powers were higher for the high HF group compared to low HF group.

While our model is the first model, to our knowledge that can produce both fast and slow spindles during UDS, previous computational models investigated the mechanism of fast spindles as well as UDS. Previous models of spindle showed that LTS properties of thalamic cells as well as

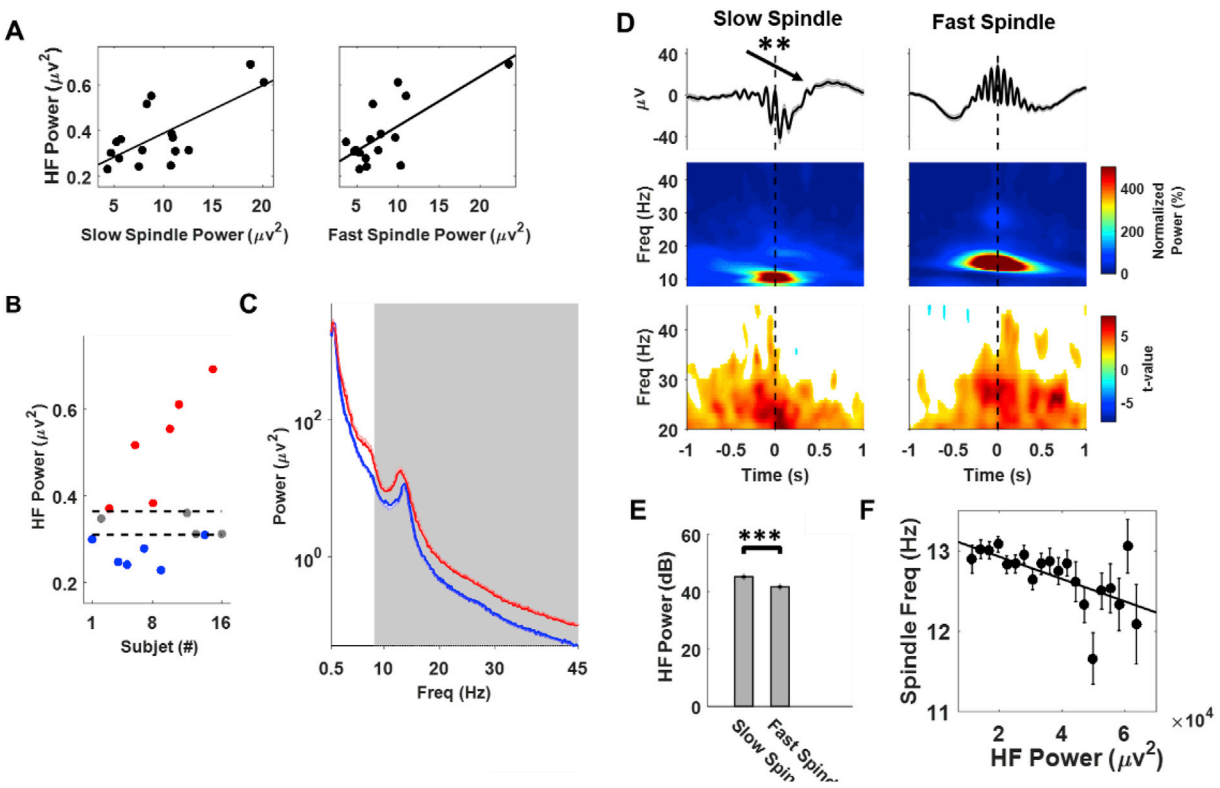

Fig. 8. Relationship between sleep oscillation and HF power over the ROI consisting of electrodes FCz and Cz. (A) Slow (8–12 Hz) and fast (12–16 Hz) spindle powers plotted versus HF (20–30 Hz) power for EEG data. Each point corresponds to a subject (the data of 16 subjects were totally used). Significant correlations ($p < 0.005$) were observed between the two pairs of variables. (B) The HF power of all 16 subjects. The red and blue dots show subjects with high and low high-frequency power during SWS, respectively while grey dots represent the excluded subjects. The dashed lines represent the fourth and fifth octiles. (C) Mean spectral power of subjects with high and low HF power are shown in red and blue, respectively. Shaded areas illustrate the frequency intervals with significant difference ($p < 0.05$) in the spectral power obtained using sliding 4 Hz windows with 90% overlap. The power at both fast and slow spindle frequency is significantly higher for the group with larger HF power (red) (D) Mean EEG (filtered below 30 Hz) time-locked to the maximum peak of slow (Left) and fast (Right) spindles (Top). A significant negative slope verified ($p < 0.005$) for the slow spindles. Slow (Left) and fast (Right) spindle event related wavelet power averaged over spindle events and subjects (Middle). t-values of the statistical comparison to baseline (Bottom, see Methods). Only values with $p < 0.05$ are shown. (E) Averaged HF power in a 1 s interval before the event of slow and fast spindles (***$p < 0.001$). (F) Spindle frequency versus averaged HF power in a 1 s interval before the spindle event (see Methods).

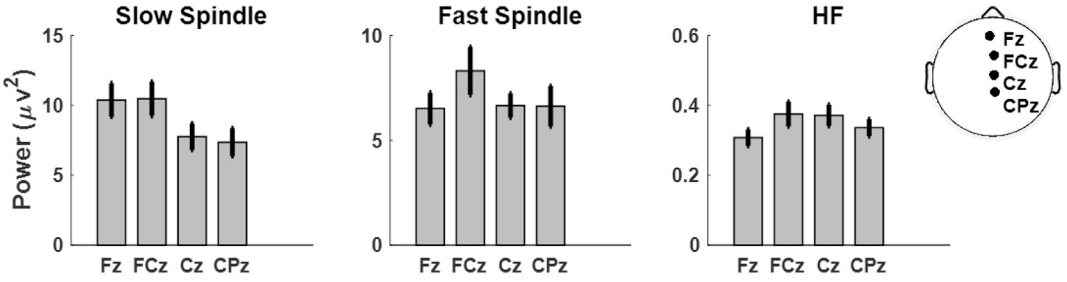

Fig. 9. Changes in the spindle and HF power from frontal to parietal electrodes. Slow spindle (Left), fast spindle (Middle) and HF (Right) power at Fz, FCz, Cz and CPz electrodes.

their interaction are sufficient to reproduce oscillations in the spindle frequency range in the isolated thalamus (Destexhe, 2009; Destexhe et al., 1996; Destexhe and Sejnowski, 2003; Timofeev and Bazhenov, 2005). Nevertheless, other mechanisms like Ca^{2+} -mediated slow regulation of the I_h current (Destexhe et al., 1993; Timofeev et al., 2001) and cortico-thalamic feedback (Bonjean et al., 2011) are necessary to take into account in order to obtain the waxing and waning envelope of spindles. Moreover, two RE and two TC recurrently connected neurons are needed to make TC neurons to generate burst of spikes every two cycles (Destexhe et al., 1996) which has been observed experimentally (Kim et al., 1995). In our model, bursting property of thalamic cells, especially TC neurons enables the isolated thalamus to generate oscillations in the frequency range of fast spindles as a result of the interaction between TC and RE neurons. This part of the model is similar to previous models (Destexhe, 2009; Izhikevich, 2007) but modified for a firing rate model. In addition, in our model, the waxing and waning envelope of fast spindle is due to cortical input to thalamic neurons. The oscillations of the order of 1 Hz representing the UDS are generated as a result of slow dynamic of DSFA similar to our previous model (Ghorbani et al., 2012). In this model the interaction between cortical inhibitory and excitatory neurons of one cortical group generates weakly underdamped harmonic oscillations during up states with a frequency roughly equal to the geometrical mean of the excitatory and inhibitory membrane time constants, which is in the range of 10–100 Hz. However, these regular oscillations change to noisy variable HF oscillations with variable duration of up and down states when two weakly coupled cortical networks are

considered instead of one uniform cortical network. Interestingly this chaotic-like dynamic is produced in the absent of any external noise or stochastic parameter, solely as a result of nonlinear interaction of weakly coupled oscillators at different frequencies. Moreover, due to DSFA, the frequency of oscillations decreases towards the end of the up state which results in higher probability of slow spindle occurrence at the end of the up state in the full thalamocortical model.

While previous studies have verified the existence of cortical beta and gamma oscillations during sleep and UDS (Compte et al., 2008; Cox et al., 2014; Le Van Quyen et al., 2010, 2016; Steriade et al., 1996; Valderrama et al., 2012), the role of these oscillations remains largely unexplored. In a relevant study, Ayoub et al. (2012) reported that EEG fast spindles were associated with MEG power in gamma frequency. However, they didn't study slow spindles and did not consider frequencies between 20 and 30 Hz. We also found distinct association of slow and fast spindles with HF oscillations by calculating the spindle event-locked power at HF and validated this prediction experimentally. The increase in the HF power before the time of slow spindle event in both model and experiment further suggests the important role of HF oscillations in the slow spindle generation. We also showed that external HF stimulation with a dominant frequency around the sum of slow and fast spindle frequencies (~ 25 Hz) boosted the slow spindle activity while HF stimulation with larger frequency did not change significantly the slow spindle activity. Future studies are required to validate this prediction of the model experimentally by applying HF stimulation during SWS. Unlike fast spindles, a distinct peak for slow spindle might be absent in the power spectrum of some subjects during SWS (Mölle et al., 2011). Our experimental results revealed that the lower slow spindle activity in these subjects was associated with lower HF power. In addition, the model predicts that the previously reported (Andrillon et al., 2011; Mölle et al., 2011) changes in the slow and fast spindle power from frontal to parietal lobe can be explained by increasing the strength of cortical excitatory neurons to thalamocortical neurons and the associated changes in the HF power. Specifically, by recording intracranial EEG in humans, a transition in slow/fast spindle activity from pSMA to SMA has been shown (Andrillon et al., 2011). In agreement with these results we also found a transition in slow/fast spindle activity around a threshold value of the strength of cortico-thalamic connections.

In our model the emergence of slow spindles is a result of the nonlinearity of the system (thalamocortical network). The nonlinearity processing at different regions of the brain has been shown in previous studies; by applying two or more stimuli with different frequencies intermodulation responses corresponding to sum or differences of the stimulus frequencies have been observed (Grossman et al., 2017; Norcia et al., 2015). While these studies focused on the intermodulation responses of external stimulus, here for the first time to our knowledge, we investigated the intermodulation frequencies of two endogenous brain oscillations, i.e. thalamic fast spindles and cortical HF oscillations.

In conclusion, we proposed a novel mechanism of slow spindle and validated it by developing a deterministic neural mass model that reproduced different experimentally observed features of both fast and slow spindles during up and down states. We further investigated the prediction of the model about the correlation between slow spindle and HF activity by recording EEG in subjects during nap. Our findings shed light on the mechanism of slow spindles by suggesting the important role of cortical HF activity in the generation of slow spindles.

Disclosure statement

This was not an industry supported study. The authors have indicated no financial conflicts of interest.

Acknowledgments

This work was supported by Iran Cognitive Sciences and Technologies Council (Project 797). We would like to thank Prof. Mayank Mehta for helpful discussions and Dr. Alireza Shadman for his assistance with the statistical analysis.

Appendix A. Supplementary data

Supplementary data to this article can be found online at https://doi.org/10.1016/j.neuroimage.2019.01.012.

References

Andrillon, T., Nir, Y., Staba, R.J., Ferrarelli, F., Cirelli, C., Tononi, G., Fried, I., 2011. Sleep spindles in humans: insights from intracranial EEG and unit recordings. J. Neurosci. 31, 17821–17834.
Ayoub, A., Aumann, D., Hörschelmann, A., Kouchekmanesch, A., Paul, P., Born, J., Marshall, L., 2013. Differential effects on fast and slow spindle activity, and the sleep slow oscillation in humans with carbamazepine and flunarizine to antagonize voltage-dependent Na+ and Ca2+ channel activity. Sleep 36, 905.
Ayoub, A., Mölle, M., Preissl, H., Born, J., 2012. Grouping of MEG gamma oscillations by EEG sleep spindles. Neuroimage 59, 1491–1500.
Barakat, M., Doyon, J., Debas, K., Vandewalle, G., Morin, A., Poirier, G., Martin, N., Lafortune, M., Karni, A., Ungerleider, L., 2011. Fast and slow spindle involvement in the consolidation of a new motor sequence. Behav. Brain Res. 217, 117–121.
Bazhenov, M., Timofeev, I., Steriade, M., Sejnowski, T.J., 2002. Model of thalamocortical slow-wave sleep oscillations and transitions to activated states. J. Neurosci. 22, 8691–8704.
Berry, R.B., Brooks, R., Gamaldo, C.E., Harding, S.M., Marcus, C., Vaughn, B., 2012. The AASM Manual for the Scoring of Sleep and Associated Events. Rules, Terminology and Technical Specifications, Darien, Illinois. American Academy of Sleep Medicine.
Bonjean, M., Baker, T., Lemieux, M., Timofeev, I., Sejnowski, T., Bazhenov, M., 2011. Corticothalamic feedback controls sleep spindle duration in vivo. J. Neurosci. 31, 9124–9134.
Buzsaki, G., 2006. Rhythms of the Brain. Oxford University Press.
Buzsáki, G., Anastassiou, C.A., Koch, C., 2012. The origin of extracellular fields and currents—EEG, ECoG, LFP and spikes. Nat. Rev. Neurosci. 13, 407–420.
Compte, A., Reig, R., Descalzo, V.F., Harvey, M.A., Puccini, G.D., Sanchez-Vives, M.V., 2008. Spontaneous high-frequency (10–80 Hz) oscillations during up states in the cerebral cortex in vitro. J. Neurosci. 28, 13828–13844.
Cona, F., Lacanna, M., Ursino, M., 2014. A thalamo-cortical neural mass model for the simulation of brain rhythms during sleep. J. Comput. Neurosci. 37, 125–148.
Costa, M.S., Weigenand, A., Ngo, H.-V.V., Marshall, L., Born, J., Martinetz, T., Claussen, J.C., 2016. A thalamocortical neural mass model of the EEG during NREM sleep and its response to auditory stimulation. PLoS Comput. Biol. 12 e1005022.
Cox, R., van Driel, J., de Boer, M., Talamini, L.M., 2014. Slow oscillations during sleep coordinate interregional communication in cortical networks. J. Neurosci. 34, 16890–16901.
Cruikshank, S.J., Urabe, H., Nurmikko, A.V., Connors, B.W., 2010. Pathway-specific feedforward circuits between thalamus and neocortex revealed by selective optical stimulation of axons. Neuron 65, 230–245.
De Gennaro, L., Ferrara, M., 2003. Sleep Spindles: an Overview. Elsevier.
Delorme, A., Makeig, S., 2004. EEGLAB: an open source toolbox for analysis of single-trial EEG dynamics including independent component analysis. J. Neurosci. Methods 134, 9–21.
Destexhe, A., 2009. Self-sustained asynchronous irregular states and up–down states in thalamic, cortical and thalamocortical networks of nonlinear integrate-and-fire neurons. J. Comput. Neurosci. 27, 493–506.
Destexhe, A., Babloyantz, A., Sejnowski, T.J., 1993. Ionic mechanisms for intrinsic slow oscillations in thalamic relay neurons. Biophys. J. 65, 1538–1552.
Destexhe, A., Bal, T., McCormick, D.A., Sejnowski, T.J., 1996. Ionic mechanisms underlying synchronized oscillations and propagating waves in a model of ferret thalamic slices. J. Neurophysiol. 76, 2049–2070.
Destexhe, A., Sejnowski, T., 2003. Interactions between membrane conductances underlying thalamocortical slow-wave oscillations. Physiol. Rev. 83, 1401–1453.
Ghorbani, M., Mehta, M., Bruinsma, R., Levine, A.J., 2012. Nonlinear-dynamics theory of up-down transitions in neocortical neural networks. Phys. Rev. 85, 021908.
Grossman, N., Bono, D., Dedic, N., Kodandaramaiah, S.B., Rudenko, A., Suk, H.-J., Cassara, A.M., Neufeld, E., Kuster, N., Tsai, L.-H., 2017. Noninvasive deep brain stimulation via temporally interfering electric fields. Cell 169, 1029–1041 e1016.
Holcman, D., Tsodyks, M., 2006. The emergence of up and down states in cortical networks. PLoS Comput. Biol. 2 e23.
Izhikevich, E.M., 2007. Dynamical Systems in Neuroscience. MIT press.
Kim, U., Bal, T., McCormick, D.A., 1995. Spindle waves are propagating synchronized oscillations in the ferret LGNd in vitro. J. Neurophysiol. 74, 1301–1323.
Klinzing, J.G., Mölle, M., Weber, F., Supp, G., Hipp, J.F., Engel, A.K., Born, J., 2016. Spindle activity phase-locked to sleep slow oscillations. Neuroimage 134, 607–616.
Le Van Quyen, M., Muller, L.E., Telenczuk, B., Halgren, E., Cash, S., Hatsopoulos, N.G., Dehghani, N., Destexhe, A., 2016. High-frequency oscillations in human and monkey neocortex during the wake–sleep cycle. Proc. Natl. Acad. Sci. Unit. States Am. 113, 9363–9368.
Le Van Quyen, M., Staba, R., Bragin, A., Dickson, C., Valderrama, M., Fried, I., Engel, J., 2010. Large-scale microelectrode recordings of high-frequency gamma oscillations in human cortex during sleep. J. Neurosci. 30, 7770–7782.
Mallat, S., 1999. A Wavelet Tour of Signal Processing. Academic press.

Mednick, S.C., McDevitt, E.A., Walsh, J.K., Wamsley, E., Paulus, M., Kanady, J.C., Drummond, S.P., 2013. The critical role of sleep spindles in hippocampal-dependent memory: a pharmacology study. J. Neurosci. 33, 4494–4504.
Mölle, M., Bergmann, T.O., Marshall, L., Born, J., 2011. Fast and slow spindles during the sleep slow oscillation: disparate coalescence and engagement in memory processing. Sleep 34, 1411–1421.
Norcia, A.M., Appelbaum, L.G., Ales, J.M., Cottereau, B.R., Rossion, B., 2015. The steady-state visual evoked potential in vision research: a review. J. Vis. 15, 4-4.
Rasch, B., Born, J., 2013. About Sleep9s role in memory. Physiol. Rev. 93, 681–766.
Sanchez-Vives, M.V., McCormick, D.A., 2000. Cellular and network mechanisms of rhythmic recurrent activity in neocortex. Nat. Neurosci. 3.
Schabus, M., Gruber, G., Parapatics, S., Sauter, C., Klösch, G., Anderer, P., Klimesch, W., Saletu, B., Zeitlhofer, J., 2004. Sleep spindles and their significance for declarative memory consolidation. Sleep 27, 1479–1485.
Sotero, R.C., Trujillo-Barreto, N.J., 2008. Biophysical model for integrating neuronal activity, EEG, fMRI and metabolism. Neuroimage 39, 290–309.
Steriade, M., Amzica, F., Contreras, D., 1996. Synchronization of fast (30-40 Hz) spontaneous cortical rhythms during brain activation. J. Neurosci. 16, 392–417.
Tallon-Baudry, C., Bertrand, O., Delpuech, C., Pernier, J., 1997. Oscillatory γ-band (30–70 Hz) activity induced by a visual search task in humans. J. Neurosci. 17, 722–734.
Timofeev, I., Bazhenov, M., 2005. Mechanisms and biological role of thalamocortical oscillations. Trends in chronobiology research 1–47.
Timofeev, I., Bazhenov, M., Sejnowski, T., Steriade, M., 2001. Contribution of intrinsic and synaptic factors in the desynchronization of thalamic oscillatory activity. Thalamus Relat. Syst. 1, 53–69.
Timofeev, I., Chauvette, S., 2013. The Spindles: Are They Still Thalamic? Oxford University Press.
Tsodyks, M.V., Markram, H., 1997. The neural code between neocortical pyramidal neurons depends on neurotransmitter release probability. Proc. Natl. Acad. Sci. Unit. States Am. 94, 719–723.
Valderrama, M., Crépon, B., Botella-Soler, V., Martinerie, J., Hasboun, D., Alvarado-Rojas, C., Baulac, M., Adam, C., Navarro, V., Le Van Quyen, M., 2012. Human gamma oscillations during slow wave sleep. PLoS One 7 e33477.